Sequential Service Restoration for Unbalanced Distribution Systems and Microgrids

Bo Chen, *Member, IEEE,* Chen Chen, *Member, IEEE,* Jianhui Wang, *Senior Member, IEEE,* and Karen L. Butler-Purry, *Senior Member, IEEE*

***Abstract*—The resilience and reliability of modern power systems are threatened by increasingly severe weather events and cyber-physical security events. An effective restoration methodology is desired to optimally integrate emerging smart grid technologies and pave the way for developing self-healing smart grids. In this paper, a sequential service restoration (SSR) framework is proposed to generate restoration solutions for distribution systems and microgrids in the event of large-scale power outages. The restoration solution contains a sequence of control actions that properly coordinate switches, distributed generators, and switchable loads to form multiple isolated microgrids. The SSR can be applied for three-phase unbalanced distribution systems and microgrids and can adapt to various operation conditions. Mathematical models are introduced for three-phase unbalanced power flow, voltage regulators, transformers, and loads. The SSR problem is formulated as a mixed-integer linear programming model, and its effectiveness is evaluated via the modified IEEE 123 node test feeder.**

***Index Terms*—Distributed generator, distribution system, microgrid, mixed-integer linear programming (MILP), restoration sequence, service restoration, self-healing**

I. Introduction

The resilience and reliability of modern power systems are threatened due to increasingly severe weather events and cyber-physical security events [1]. Major storms and sophisticated cyber-physical attacks can result in tremendous loss of life, destruction of property, and large-scale power outages which may last hours or even days [2-4]. To expedite the restoration progress, many efforts have been made toward developing self-healing smart grids with features that can automatically identify, isolate, and restore the problematic elements with few, if any, manual interruptions [5]. Specifically, emerging smart grid technologies are playing more and more important roles in fast service restoration for both transmission and distribution systems [6, 7]. For example, in distribution systems, remotely controllable switches (e.g., sectionalizing switches, tie switches) enable the post-fault network reconfiguration, which provides alternative energization paths for the affected loads [8-11]; distributed energy resources (DERs) and microgrids can support load demands locally during the restoration to release the line capacity and improve the voltage profile [12-19].

The distribution service restoration (DSR) problem is traditionally formulated as a combinatorial optimization problem, and has been well studied in the literature [8-11]. Conventional service restoration is implemented through reconfiguration. By introducing distributed generators (DGs) and microgrids, the DSR model can be adapted by assuming their output power as being the negative constant load, or dispatching DGs and microgrids while searching for the optimized configuration [12-15]. Recently, researchers have proposed various methods to partition the distribution systems into isolated subsystems based on the concept of the microgrid. The load demand within each isolated microgrid can be balanced by the DGs within the same microgrid [16-18]. However, most existing algorithms in the literature formulate the DSR problem as a single-step optimization problem, which can only provide a final configuration. Single-step methods do not consider the task of generating an intermediate feasible restoration sequence, which the system operators desire in order to restore the system from a post-fault configuration to the final configuration. Various algorithms have been proposed to determine the switching sequence, such as genetic algorithm [20], dynamic programming [21], mixed-integer programming (MIP) [22, 23], and branch and bound algorithm [15]. In the distribution control center, switching order management (SOM) software is normally used to generate and validate the switching sequences [24]. Existing sequence-generating algorithms work well for conventional distribution systems without DERs. Integrating the operation of DERs into the DSR problem introduces both unprecedented opportunities and challenges for generating restoration sequences in the context of active distribution systems and microgrids. Specifically, DERs should be properly coordinated to share the load demand while satisfying various operation constraints throughout the restoration process. Single-step methods cannot handle inter-temporal constraints that involve multiple time steps (e.g., ramp rate constraint for dispatchable DGs). Therefore, the final configuration provided by the single-step methods may be invalid, if a feasible restoration sequence cannot be generated. An algorithm that can fully coordinate the DG dispatching actions and the switching actions during the restoration process is presented in this paper.

Distribution systems are inherently unbalanced given that the load demands on each phase are always changing randomly [25]. However, most papers assume the distribution systems under study are three-phase balanced. Some algorithms can be easily adapted to incorporate unbalanced operational conditions such

B. Chen is with the Energy Systems Division, Argonne National Laboratory, Argonne, IL 60439 USA (e-mail: bo.chen@anl.gov). He was with the Department of Electrical and Computer Engineering, Texas A&M University, College Station, TX 77840 USA.

C. Chen is with the Energy Systems Division, Argonne National Laboratory, Argonne, IL 60439 USA (e-mail: morningchen@anl.gov).

J. Wang is with the Department of Electrical Engineering at Southern Methodist University, Dallas, TX, USA and the Energy Systems Division at Argonne National Laboratory, Argonne, IL, USA (email: jianhui.wang@ieee.org)

K. L. Butler-Purry is with the Department of Electrical and Computer Engineering, Texas A&M University, College Station, TX 77840 USA (e-mail: klbutler@tamu.edu).

as heuristic algorithms and rule-based expert system algorithms [26, 27]. But they may not guarantee finding the globally optimal solution. In order to improve the optimality, some linear three-phase power flow equations have been proposed in the literature [28-31]. They can potentially be incorporated into the problem formulation for distribution system applications such as optimal power flow, reconfiguration, and service restoration. In addition, various components in typical distribution systems and microgrids such as voltage regulators, transformers, and ZIP loads (i.e., constant impedance (Z), constant current (I), and constant power (P)) should be considered [28]. Furthermore, the DGs under unbalanced operation conditions are subjected to various constraints (e.g., current unbalance constraint, ramping rate constraint, and output limit constraint), thereby introducing additional challenges for problem formulation [32].

To address the aforementioned challenges, this paper proposes a sequential service restoration (SSR) framework for radial distribution systems and microgrids with dispatchable DGs. The main contributions of this paper are to:

1. Develop a SSR framework to generate restoration sequences that could fully coordinate the operation of DGs and switchgears over multiple time steps.
2. Introduce a system model that incorporates linear three-phase power flow, ZIP loads, voltage regulators, transformers, capacitor banks, and DG unbalanced operation conditions.
3. Formulate the SSR problem as a mixed-integer linear programming (MILP) model which could be effectively solved by off-the-shelf MILP solvers.
4. Propose a set of topological and sequencing constraints based on the concept of the "bus block," which can partition the system into multiple isolated subsystems while maintaining the tree structure.

The remainder of this paper is organized as follows. Section II introduces the SSR methodology. Section III introduces the MILP model for SSR. Section IV provides numerical results, and conclusions are discussed in Section V.

II. SSR Methodology

Emerging DGs and various remotely controllable devices in modern distribution systems demonstrate great potential that can be leveraged for service restoration. The proposed SSR aims to advance the conventional service restoration technique by coordinating these emerging techniques to achieve more efficient restoration solutions. More specifically, the proposed SSR will generate a sequence of control actions that optimally coordinate DGs and switchgears to restore as much load demand as possible. The control actions are assigned to multiple time steps, and at each time step, various operational constraints are satisfied to guarantee that the restoration solution can be implemented successfully. Note that most distribution systems are constructed in weakly meshed topology and operated in radial topology, because it is easier to implement fault location, isolation, and protection coordination [25]. However, radially operated distribution systems are no longer radial after introducing a high penetration of DGs that can cause bidirectional power flow [33]. In this paper, we assume that radial distribution systems and microgrids with multiple DGs are operated in tree topology. Unlike radial operation, which requires unidirectional power flow, tree topology allows bidirectional power flow and maintains radial structure [34].

The SSR methodology can be implemented by performing the following steps.

Step 1) *Information Collection*. The outage management system (OMS) collects data from various types of entities such as the customer information system (CIS), interactive voice response (IVR), advanced metering infrastructure (AMI), and the field measurements (e.g., protective relays, fault indicators, switchgears) through the supervisory control and data acquisition (SCADA) system.

Step 2) *Fault Location and Isolation*. After being hit by severe weather events, a power system can be subjected to multiple faults that occur at different components and locations. Based on the information collected from the protective relays and fault indicators, the fault locations can be pinpointed. The faulty areas can be isolated by opening the switches that are installed along the feeders. Then the maintenance crews are dispatched to fix the failed components in the isolated faulty areas.

Step 3) *System Model Identification*. The resources that can potentially participate in the restoration are determined in this step by assessing the availability and controllability of various components such as DGs, lines, switches, and loads.

Step 4) *Service Restoration*. The proposed SSR algorithm is performed by solving the MILP model and generating a restoration sequence that can coordinate all the controllable components across multiple time steps. Then the system can be sequentially restored. If the restoration sequence cannot be successfully carried out (e.g., loss of communication, or damaged by succeeding outages), system operators should return to Step (1) to collect up-to-date information, isolate the problematic components in Step (2), update the system model in Step (3), and generate a new restoration sequence in Step (4).

III. MILP Formulation for SSR

In this section, the sets and decision variables are defined, and then the MILP formulation is presented. Specifically, the mathematical models of various power system components (e.g., voltage regulator, transformer, ZIP load) and operational constraints are introduced.

A. Model Representation

A series of sets is defined to represent the components (e.g., nodes, lines, loads, DGs) based on their controllability status. A distribution system consists of N_n buses, N_{br} lines, N_l loads, and N_g DGs, where $\mathcal{N} \coloneqq \{1,2,\dots,N_n\}$ represents the set of all the buses such as load buses and DG buses. $\mathcal{L} \subseteq \mathcal{N}$ is the set of buses connected to loads. $\mathcal{G} \subseteq \mathcal{N}$ is the set of substation buses and buses connected to dispatchable DGs. Then, $\mathcal{B} \coloneqq \{(i,j): i \in \mathcal{N}, j \in \mathcal{N},\ i \neq j\}$ represents the set of all the lines in the system, and $\mathcal{V} \subseteq \mathcal{B}$ denotes the set of lines installed with voltage regulators and transformers.

The superscript "S" represents the controllability of a component. Namely, $\mathcal{B}^S \subseteq \mathcal{B}$ is the set of lines that can be

remotely controlled; $\mathcal{L}^S \subseteq \mathcal{L}$ is the set of loads that can be remotely switched on or off; $\mathcal{G}^S \subseteq \mathcal{G}$ is the set of substation buses (i.e., slack buses) or DGs with black start capability. It is worth mentioning that the dispatchable DGs without black start capability can only be started from external sources.

Similarly, the superscript "F" represents the failure status of the components. Namely, $\mathcal{N}^F \subseteq \mathcal{N}$ is the set of nodes that cannot be energized (e.g., fallen power poles, flooded substations); $\mathcal{B}^F \subseteq \mathcal{B}$ is the set of lines that are damaged or disconnected (e.g., trees lean on these lines, blown fuses); $\mathcal{L}^F \subseteq \mathcal{L}$ is the set of loads that cannot be restored in a short time; $\mathcal{G}^F \subseteq \mathcal{G}$ is the set of DGs that cannot be utilized for service restoration.

Next, $\mathcal{T} \coloneqq \{1,2,\dots,T\}$ is the set of steps. T is the length of horizon and Δt is the length of each step. A set of binary variables and continuous variables is defined to represent the control actions and energization statuses of various components at each step $t \in \mathcal{T}$. Namely, $s_{i,t}^N \in \{0,1\}$ represents the energization status of node i at step t; $x_{ij,t}^{BR} \in \{0,1\}$ determines whether the line (i,j) is energized at step t; $x_{l,t}^L \in \{0,1\}$ determines whether the load l is restored at step t; and $x_{g,t}^G \in \{0,1\}$ determines whether the DG g is started at step t. $P_{g,t}^{\phi} \in \mathbb{R}$ and $Q_{g,t}^{\phi} \in \mathbb{R}$ are defined as the active and reactive power provided by the DG at node $g \in \mathcal{G}$ for each phase at step t. $\phi \in \Phi \coloneqq \{a,b,c\}$ represents the phases. These binary and continuous variables are the decision variables of the MILP model, and the restoration solutions could be generated based on their values, as shown in Fig. 1.

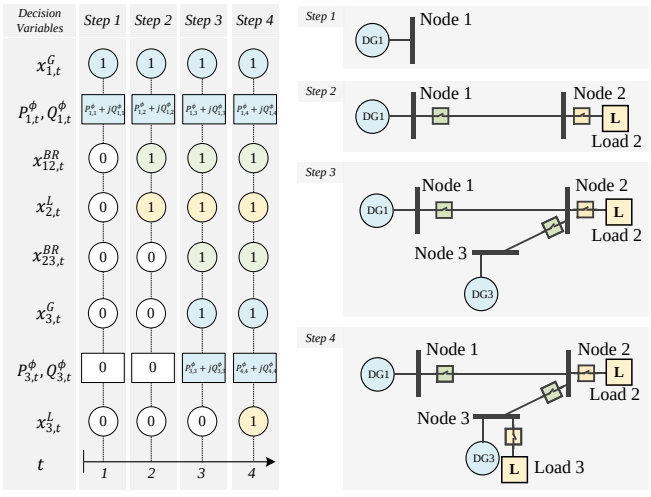

Fig. 1. Possible restoration sequence derived from the binary variables and continuous variables that are solved by the proposed DSR model: (a) decision variables, (b) derived restoration sequence.

Fig. 1 shows an example of how to derive the restoration sequence for a simple three-node system, which could be a distribution system or a microgrid. Components are numbered according to the node number. All lines and loads are assumed to be switchable and disconnected at Step 1. DG1 is a black start DG, and DG2 is a dispatchable DG without black start capability. A possible restoration solution, which is assumed to be generated by the proposed SSR method, is shown in Fig. 1(a). At each step, the energization status of each component is shown. The active and reactive power output of each energized DG is shown as well. If two or more DGs are energized, they will be cooperatively dispatched. Fig. 1(b) shows the configurations of the energized system at each step. At Step 1, $x_{1,1}^G = 1$, meaning DG1 is started to energize Node 1. At Step 2, $x_{12,2}^{BR} = 1$, meaning the switchable line between Node 1 and Node 2 is closed to energize Node 2, which further enables Load 2 to be energized (i.e., $x_{2,2}^L = 1$). Similarly, Node 3 is energized at Step 3 by closing the line between Node 2 and Node 3. Meanwhile, DG3 is started to share the load demand, since its terminal node (i.e., Node 3) is energized. The proposed SSR method should coordinate all the controllable components to restore as much load as possible across multiple steps, and ensure all the constraints are satisfied.

B. Objective Function

The objective function is defined to maximize the total restored energy over the time horizon considering the weight factor of each load l (denoted as β_l^L):

$$\max \sum_{l\in\mathcal{L}} \sum_{t\in\mathcal{T}} \sum_{\phi\in\{a,b,c\}} \beta_l^L \cdot P_{l,t}^{\phi} \cdot \Delta t, \qquad (1)$$

and subject to the following constraints:

1) System model constraints ((8)–(9) and (16))
2) System operation constraints ((19) – (22))
3) DG operation constraints ((26) – (28))
4) Connectivity constraints ((29) – (31))
5) Topological and sequencing constraints ((32) – (33))

The problem is formulated as a MILP model, which can be solved effectively by off-the-shelf solvers such as CPLEX.

C. System Model Constraints

1) Linear three-phase power flow model

Many smart grid applications integrated in a modern distribution management system (DMS) require the power flow to be calculated in real time or near real time. Linear power flow is a powerful tool that can be easily incorporated into the models of various applications. A linear power flow model for three-phase unbalanced systems is proposed in [28-31] and introduced as follows.

For each line $(i,j) \in \mathcal{B}$, we apply Kirchhoff's voltage law, and then we have [25]:

$$\boldsymbol{V}_j = \boldsymbol{V}_i - \boldsymbol{z}_{ij}\boldsymbol{I}_{ij}, \qquad (2)$$

where $\boldsymbol{V}_i = \left[V_i^a, V_i^b, V_i^c\right]^{\mathrm{T}} \in \mathbb{C}^{3\times 1}$ is the vector of complex numbers representing three-phase voltage at bus i. $\boldsymbol{V}_j = \left[V_j^a, V_j^b, V_j^c\right]^{\mathrm{T}} \in \mathbb{C}^{3\times 1}$, $\boldsymbol{I}_{ij} = \left[I_{ij}^a, I_{ij}^b, I_{ij}^c\right]^{\mathrm{T}} \in \mathbb{C}^{3\times 1}$, and $\boldsymbol{z}_{ij} \in \mathbb{C}^{3\times 3}$ is the total line impedance consisting of resistance $\boldsymbol{r}_{ik}$ and reactance $\boldsymbol{x}_{ij}$, which are determined by the phase impedance matrix $\boldsymbol{z}_{ij}^{abc} \in \mathbb{C}^{3\times 3}$ in Ω/mile and the length of the line $l(i,j)$ in miles [25]:

$$\boldsymbol{z}_{ij} = l(i,j)\boldsymbol{z}_{ij}^{abc} = \boldsymbol{r}_{ij} + \mathrm{j}\boldsymbol{x}_{ij}. \qquad (3)$$

Note "j" is used to denote the node index, and "j" is used to denote the imaginary part of a complex number.

Denoting $\odot$ and $\oslash$ as the element-wise product and division, respectively, the line current $\boldsymbol{I}_{ij}$ can be calculated by

$$\boldsymbol{I}_{ij} = \boldsymbol{S}_{ij}^* \oslash \boldsymbol{V}_i^*, \qquad (4)$$

where $\boldsymbol{S}_{ij} = \left[P_{ij}^a + \mathrm{j}Q_{ij}^a, P_{ij}^b + \mathrm{j}Q_{ij}^b, P_{ij}^c + \mathrm{j}Q_{ij}^c\right]^{\mathrm{T}} \in \mathbb{C}^{3\times 1}$ is the apparent power from bus i to bus j. Substituting (4) into (2) and

multiplying the left side and the right side by their complex conjugate, respectively [30], we have:

$$\boldsymbol{V}_j \odot \boldsymbol{V}_j^* = \boldsymbol{V}_i \odot \boldsymbol{V}_i^* - \boldsymbol{z}_{ij}(\boldsymbol{S}_{ij}^* \oslash \boldsymbol{V}_i^*) \odot \boldsymbol{V}_i^* - \boldsymbol{z}_{ij}^*(\boldsymbol{S}_{ij} \oslash \boldsymbol{V}_i) \odot \boldsymbol{V}_i + \boldsymbol{c}_{ij}(\boldsymbol{S}_{ij}, \boldsymbol{V}_i, \boldsymbol{z}_{ij}), \quad (5)$$

where $\boldsymbol{c}_{ij}(\boldsymbol{S}_{ij}, \boldsymbol{V}_i, \boldsymbol{z}_{ij})$ is the higher-order term which can be neglected if the line losses is small compared to power flow and voltages are nearly balanced [29]:

$$\frac{V_i^a}{V_i^b} \approx \frac{V_i^b}{V_i^c} \approx \frac{V_i^c}{V_i^a} \approx e^{\mathrm{j}2\pi/3}. \quad (6)$$

Note that (6) only holds for three-phase buses. For two-phase buses, only presenting phases are assumed to be nearly balanced. Substituting (6) into (5), denoting $\boldsymbol{U} = [|V^a|^2, |V^b|^2, |V^c|^2]^T$ and neglecting $\boldsymbol{c}_{ij}$, we have:

$$\boldsymbol{U_j} = \boldsymbol{U_i} - \widetilde{\boldsymbol{z}}_{ij}\boldsymbol{S}_{ij}^* - \widetilde{\boldsymbol{z}}_{ij}^*\boldsymbol{S}_{ij}, \quad (7)$$

where $\widetilde{\boldsymbol{z}}_{ij} = \boldsymbol{\alpha} \odot \boldsymbol{z}_{ij} \in \mathbb{C}^{3\times 3}$, and $\boldsymbol{\alpha}$ is defined as:

$$\boldsymbol{\alpha} = \begin{bmatrix} 1 & e^{-\mathrm{j}2\pi/3} & e^{\mathrm{j}2\pi/3} \\ e^{\mathrm{j}2\pi/3} & 1 & e^{-\mathrm{j}2\pi/3} \\ e^{-\mathrm{j}2\pi/3} & e^{\mathrm{j}2\pi/3} & 1 \end{bmatrix}.$$

Together with the power balance constraints for each bus at each step, we can formulate the linear power flow constraints considering the energization status of each line at each step:

$$\boldsymbol{U}_{i,t} - \boldsymbol{U}_{j,t} \le \widetilde{\boldsymbol{z}}_{ij}\boldsymbol{S}_{ij,t}^* + \widetilde{\boldsymbol{z}}_{ij}^*\boldsymbol{S}_{ij,t} + M\left(1 - x_{ij,t}^{BR}\right)\boldsymbol{e}_{\boldsymbol{ij}}^{\phi}, \quad (8a)$$

$$\boldsymbol{U}_{i,t} - \boldsymbol{U}_{j,t} \ge \widetilde{\boldsymbol{z}}_{ij}\boldsymbol{S}_{ij,t}^* + \widetilde{\boldsymbol{z}}_{ij}^*\boldsymbol{S}_{ij,t} - M\left(1 - x_{ij,t}^{BR}\right)\boldsymbol{e}_{\boldsymbol{ij}}^{\phi}, \quad (i,j) \in B \backslash \mathcal{V}, t \in \mathcal{T}, \quad (8b)$$

$$\sum_{h:(h,i)\in B} \boldsymbol{P}_{hi,t}^{BR} + \sum_{g:g=i,g\in\mathcal{G}} \boldsymbol{P}_{g,t}^{G} = \sum_{j:(i,j)\in B} \boldsymbol{P}_{ij,t}^{BR} + \sum_{l:l=i,l\in\mathcal{L}} \boldsymbol{P}_{l,t}^{L}, \quad (8c)$$

$$\sum_{h:(h,i)\in B} \boldsymbol{Q}_{hi,t}^{BR} + \sum_{g:g=i,g\in\mathcal{G}} \boldsymbol{Q}_{g,t}^{G} = \sum_{j:(i,j)\in B} \boldsymbol{Q}_{ij,t}^{BR} + \sum_{l:l=i,l\in\mathcal{L}} \boldsymbol{Q}_{l,t}^{L}, (i,j) \in B, t \in \mathcal{T}, \quad (8d)$$

where $\boldsymbol{e}_{\boldsymbol{ij}}^{\phi} \in \{0,1\}^{3\times 1}$ is the vector with binary entries to represent phases. For example, if a branch (i,j) is a single-phase line (e.g., phase B), then $\boldsymbol{e}_{\boldsymbol{ij}}^{\phi} = [0,1,0]^T$. $(\boldsymbol{P}_{ij,t}^{BR} + \mathrm{j}\boldsymbol{Q}_{ij,t}^{BR})$ is the vector of three-phase apparent power flowing from bus i to bus j through line (i,j) at step t. $(\boldsymbol{P}_{g,t}^{G} + \mathrm{j}\boldsymbol{Q}_{g,t}^{G})$ is the three-phase power outputted by DG g at step t. $(\boldsymbol{P}_{l,t}^{L} + \mathrm{j}\boldsymbol{Q}_{l,t}^{L})$ is the three-phase load demand on node l at step t. The big-M method is used in (8a)–(8b) to ensure that the equality constraints are only applied for energized lines, except voltage regulators and transformers [35]. M is a large number and should be selected carefully to ensure that the constraints are valid only when the line is energized. Active and reactive power balance at each node is guaranteed by (8c)–(8d).

The linear models for voltage regulators, transformers, ZIP loads, and capacitor banks are introduced below.

2) Voltage regulator and transformer models

A single-phase voltage regulator can be modeled as an ideal transformer connected with an equivalent line representing the leakage impedance [36]. A three-phase voltage regulator can be modeled by connecting three single-phase voltage regulators. Transformers share the same model as voltage regulators but with fixed ratios. In this paper, all of the regulators are assumed to be wye-connected type B regulators. A linear voltage regulator model is proposed in [36].

The relationship between the voltage magnitudes on both sides for a three-phase voltage regulator, with i as the primary side and j as the secondary side, can be expressed as:

$$-M\left(1 - x_{ij,t}^{BR}\right)\boldsymbol{e}_{\boldsymbol{ij}}^{\phi} \le \boldsymbol{a}^2 \odot \boldsymbol{U}_j - \boldsymbol{U}_i \le M\left(1 - x_{ij,t}^{BR}\right)\boldsymbol{e}_{\boldsymbol{ij}}^{\phi}, (i,j) \in \mathcal{V}, t \in \mathcal{T}, \quad (9)$$

where $\boldsymbol{a} \in \mathbb{R}^{3\times 1}$ is the vector representing the ratio between secondary winding and primary winding for each phase. Again, M is a large number that should be selected carefully. The regulator is assumed to be adjustable from −16 step to +16 step, in order to regulate the voltage from +10% to −10%, with 5/8% per step [25]. Denoting $\boldsymbol{n^{tap}} \in \{-16, -15, \dots, +15, +16\}$ as the tap position for each phase, the ratio is calculated by:

$$\boldsymbol{a} = 1 + 0.00625\boldsymbol{n^{tap}}. \quad (10)$$

Note that the tap positions are assumed to be fixed in this paper. However, tap positions can be modeled as decision variables and incorporated into the proposed SSR framework using the linear model proposed in [37].

3) ZIP loads and capacitor banks models

All the loads are assumed to be voltage-dependent loads, which are normally modeled by the composite of constant impedance (Z), constant current (I), and constant power (P and Q). For each phase, the voltage-dependent load demand $(P_l + \mathrm{j}Q_l)$ for load $l \in \mathcal{L}$ can be described as:

$$\frac{P_l}{P_l^N} = a_{l,p}^Z \left(\frac{|V_l|}{|V_l^N|}\right)^2 + a_{l,p}^I \left(\frac{|V_l|}{|V_l^N|}\right) + a_{l,p}^P, \quad (11a)$$

$$\frac{Q_l}{Q_l^N} = a_{l,q}^Z \left(\frac{|V_l|}{|V_l^N|}\right)^2 + a_{l,q}^I \left(\frac{|V_l|}{|V_l^N|}\right) + a_{l,q}^P, \quad (11b)$$

where $P_l^N + \mathrm{j}Q_l^N$ is the load demand of load l at the nominal voltage V_l^N; $a_{l,p}^Z$, $a_{l,p}^I$, $a_{l,p}^P$, $a_{l,q}^Z$, $a_{l,q}^I$, and $a_{l,q}^P$ are coefficients representing the percentages of constant impedance, current, and power of active and reactive power of load l, and should satisfy:

$$a_{l,p}^Z + a_{l,p}^I + a_{l,p}^P = 1, a_{l,q}^Z + a_{l,q}^I + a_{l,q}^P = 1, \quad (12a)$$

$$a_{l,p}^Z, a_{l,p}^I, a_{l,p}^P, a_{l,q}^Z, a_{l,q}^I, a_{l,q}^P \in \mathbb{R}_{\ge 0}. \quad (12b)$$

Substituting $U_{l,t} = \left|V_{l,t}\right|^2$ into the above equations while considering the energization status of load l at step t, the single-phase load demand at each step can be expressed by two nonlinear functions of $U_{l,t}$ and $x_{l,t}^L$:

$$P_{l,t} = x_{l,t}^L P_l^N \left(\frac{a_{l,p}^Z}{|V_l^N|^2} U_{l,t} + \frac{a_{l,p}^I}{|V_l^N|}\sqrt{U_{l,t}} + a_{l,p}^P\right), \quad (13a)$$

$$Q_{l,t} = x_{l,t}^L Q_l^N \left(\frac{a_q^Z}{|V_l^N|^2} U_{l,t} + \frac{a_{l,q}^I}{|V_l^N|}\sqrt{U_{l,t}} + a_{l,q}^P\right). \quad (13b)$$

Considering $U_{l,t}$ varies in a small range when the node is energized and is constrained by the voltage magnitude constraint, the nonlinear term $\sqrt{U_{l,t}}$ can be linearized around $U_{l,t} = 1.0$ based on its Taylor series expansion:

$$\sqrt{U_{l,t}} \approx 0.5 + 0.5U_{l,t}. \quad (14)$$

Substituting (14) into (13), we have:

$$P_{l,t} = P_l^N \left(\frac{a_{l,p}^Z}{|V_l^N|^2} + 0.5\frac{a_{l,p}^I}{|V_l^N|}\right) x_{l,t}^L U_{l,t} + P_l^N \left(0.5\frac{a_{l,p}^I}{|V_l^N|} + a_{l,p}^P\right) x_{l,t}^L, \quad (15a)$$

$$Q_{l,t} = Q_l^N \left(\frac{a_{l,q}^Z}{|V_l^N|^2} + 0.5\frac{a_{l,q}^I}{|V_l^N|}\right) x_{l,t}^L U_{l,t} + Q_l^N \left(0.5\frac{a_{l,q}^I}{|V_l^N|} + a_{l,q}^P\right) x_{l,t}^L. \quad (15b)$$

The nonlinear term $x_{l,t}^L U_l$ can be linearized by introducing an extra variable $y_{l,t}$ and two extra inequality constraints (i.e., (16c) and (16d)). Then, the three-phase wye-connected load at step t can be described as:

$$\boldsymbol{P}_{l,t}^L = \boldsymbol{P}_l^{LN} \odot \left(\frac{a_{l,p}^Z}{|V_l^N|^2} + 0.5\frac{a_{l,p}^I}{|V_l^N|}\right) \boldsymbol{y}_{l,t} + \boldsymbol{P}_l^{LN} \left(0.5\frac{a_{l,p}^I}{|V_l^N|} + a_{l,p}^P\right) x_{l,t}^L, \quad (16a)$$

$$\boldsymbol{Q}_{l,t}^L = \boldsymbol{Q}_l^{LN} \odot \left(\frac{a_{l,q}^Z}{|V_l^N|^2} + 0.5\frac{a_{l,q}^I}{|V_l^N|}\right) \boldsymbol{y}_{l,t} + \boldsymbol{Q}_l^{LN} \left(0.5\frac{a_{l,q}^I}{|V_l^N|} + a_{l,q}^P\right) x_{l,t}^L, \quad (16b)$$

$$\boldsymbol{0} \le \boldsymbol{y}_{l,t} \le x_{l,t}^L \boldsymbol{U}_{max}, \quad (16c)$$

$$(1-x_{l,t}^{L})\boldsymbol{U}^{min} \le \boldsymbol{U}_{l,t} - \boldsymbol{y}_{l,t} \le (1-x_{l,t}^{L})\boldsymbol{U}^{max}, \quad (16d)$$

where $\boldsymbol{P}_l^{LN} = \left[P_l^{aN}, P_l^{bN}, P_l^{cN}\right]^T$, $\boldsymbol{Q}_l^{LN} = \left[Q_l^{aN}, Q_l^{bN}, Q_l^{cN}\right]^T$, $\boldsymbol{y}_{l,t} = \left[y_{l,t}^a, y_{l,t}^b, y_{l,t}^c\right]^T$. $\boldsymbol{U}^{min}$ and $\boldsymbol{U}^{max}$ are set to $0.95^2\ p.u.$ and $1.05^2\ p.u.$, respectively, for each presenting phase. In this paper, for each load, the same ZIP parameters and nominal voltage are used for each presenting phase.

For delta-connected loads as shown in Fig. 2, the approximated wye-connected model can be derived by assuming (6) still holds. For the approximated load on phase A, we have:

$$S_a^L = V_a I_a^* = V_a\left(\frac{S_{ab}^L}{V_{ab}} - \frac{S_{ca}^L}{V_{ca}}\right) \approx \frac{e^{-\mathrm{j}\pi/6}}{\sqrt{3}} S_{ab}^L - \frac{e^{-\mathrm{j}5\pi/6}}{\sqrt{3}} S_{ca}^L. \quad (17)$$

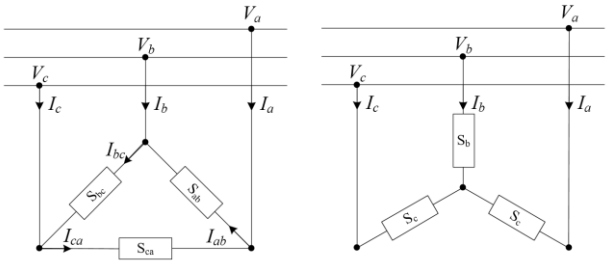

Fig. 2. The approximated wye-connected model of a delta-connected load: (a) delta-connected load, (b) approximated wye-connected load.

Similarly, we can derive S_b^L and S_c^L and derive the approximated wye-connected load in matrix form:

$$\begin{bmatrix} S_a^L \\ S_b^L \\ S_c^L \end{bmatrix} = \frac{1}{\sqrt{3}} \begin{bmatrix} e^{-\frac{\mathrm{j}\pi}{6}} & 0 & -e^{-\frac{\mathrm{j}5\pi}{6}} \\ -e^{-\frac{\mathrm{j}5\pi}{6}} & e^{-\frac{\mathrm{j}\pi}{6}} & 0 \\ 0 & -e^{-\frac{\mathrm{j}5\pi}{6}} & -e^{-\frac{\mathrm{j}\pi}{6}} \end{bmatrix} \begin{bmatrix} S_{ab}^L \\ S_{bc}^L \\ S_{ca}^L \end{bmatrix}. \quad (18)$$

Note that the same ZIP parameters are applied for $S_{ab}^L, S_{bc}^L, S_{ca}^L$. Single-phase and two-phase loads in both wye connection and delta connection can be modeled in a similar way by setting the variables associated with the missing phase(s) to zero. Wye-connected and delta-connected capacitor banks are modeled as switchable constant impedance loads.

Equations (8)–(9) and (16) form the linear power flow for unbalanced three-phase power systems with DGs, voltage regulators, transformers, capacitor banks, and ZIP loads.

D. System Operation Constraints

1) Transformer and line capacity constraints

$$\boldsymbol{0} \le \boldsymbol{P}_{ij,t}^{BR} \le \boldsymbol{P}_{ij}^{max} \cdot x_{ij,t}^{BR}, (i,j) \in \mathcal{B}, t \in \mathcal{T}, \quad (19a)$$

$$\boldsymbol{0} \le \boldsymbol{Q}_{ij,t}^{BR} \le \boldsymbol{Q}_{ij}^{max} \cdot x_{ij,t}^{BR}, (i,j) \in \mathcal{B}, t \in \mathcal{T}, \quad (19b)$$

where P_{ij}^{max} and Q_{ij}^{max} are maximum permissive active and reactive power. Equations (19a)–(19b) ensure that the line power on each presenting phase is zero if this line is not energized, and should be maintained within the permissive range if this line is energized.

2) Voltage limit constraints

$$s_{i,t}^N \cdot \boldsymbol{U}^{min} \le \boldsymbol{U}_{i,t} \le s_{i,t}^N \cdot \boldsymbol{U}^{max}, \quad i \in \mathcal{N}, t \in \mathcal{T}, \quad (20)$$

where $\boldsymbol{U}_{i,t} = [\left|V_{i,t}^a\right|^2, \left|V_{i,t}^b\right|^2, \left|V_{i,t}^c\right|^2]^T$.

3) Maximum load step constraints

To allow the voltage and frequency of each isolated microgrid to recover quickly, picking up large block loads at a time should be avoided [38]. For each DG, a maximum load step (MLS) factor is defined as a fraction of the rated DG capacity. Then, the incremental loading on each DG at each step should be smaller than the maximum permissive step load.

$$\sum_{\phi\in\{a,b,c\}} P_{g,t}^{\phi} - \sum_{\phi\in\{a,b,c\}} P_{g,t-1}^{\phi} \le MLS \cdot P_g^{Cap}, \quad g \in \mathcal{G}, t \in \mathcal{T}, t > 1, \quad (21)$$

where P_g^{Cap} is the rated capacity of DG g. Note that the MLS factor should be carefully approximated for each DG. In this paper, it is assumed that the DGs, transformers, lines, and associated protective relays can withstand the transient inrush current induced by the cold load pickup issues.

4) Initial condition constraints

The initial conditions are defined by directly assigning values to the corresponding binary decision variables based on the information collected from the devices at the post-outage stage. Specifically, substation buses and black start DGs are started from the first step, and the voltage is maintained at 1.0 p.u. All the switchable lines are opened at the first step.

$$x_{g,t}^G = 1, \boldsymbol{U}_g^2 = [1.0, 1.0, 1.0]^T, g \in \mathcal{G}^S \backslash \mathcal{G}^F, t \in \mathcal{T}, \quad (22a)$$

$$x_{ij,t}^{BR} = 0,\ (i,j) \in \mathcal{B}^S \backslash \mathcal{B}^F, t = 1. \quad (22b)$$

For components that cannot participate in the restoration, the binary variables are set to zero.

$$x_{ij,t}^{BR} = 0, x_{g,t}^G = 0, s_{k,t}^N = 0, x_{l,t}^L = 0, (i,j) \in \mathcal{B}^F, g \in \mathcal{G}^F, k \in \mathcal{N}^F, l \in \mathcal{L}^F, t \in \mathcal{T}. \quad (22c)$$

E. DG Operation Constraints

1) DG current unbalance constraints

Three-phase DGs under unbalanced operation conditions should satisfy the current unbalance constraint to avoid overheating [39]. A current unbalance factor (CUF) is defined as the ratio of negative sequence current ($I_2^{(1)}$) to positive sequence current ($I_1^{(1)}$) at the first harmonic:

$$CUF = \frac{\left|I_2^{(1)}\right|}{\left|I_1^{(1)}\right|}, \quad (23)$$

$$I_2^{(1)} = (I^a + \alpha^2 I^b + \alpha I^c)/3,\ I_1^{(1)} = (I^a + \alpha I^b + \alpha^2 I^c)/3, \quad (19b)$$

where $\alpha = e^{\mathrm{j}2\pi/3}$. Three-phase synchronous DGs will trip when CUF exceeds 10%–20%. Inverter-based DG can operate up to 100% CUF [39].

Substituting (4) into (23), assuming (6) holds, we have [32]:

$$CUF \approx \frac{\left|S^a + \alpha^2 S^b + \alpha S^c\right|}{\left|S^a + S^b + S^c\right|} = \frac{\left|P^N + jQ^N\right|}{\left|P^P + jQ^P\right|}. \quad (24)$$

A simple function introduced in [40] is used to approximate (24). Letting $S_{g,t}^a + \alpha^2 S_{g,t}^b + \alpha S_{g,t}^c = P_{g,t}^N + \mathrm{j}Q_{g,t}^N$, $S_{g,t}^a + S_{g,t}^b + S_{g,t}^c = P_{g,t}^P + \mathrm{j}Q_{g,t}^P$, we have:

$$\frac{\left|P_{g,t}^N + \mathrm{j}Q_{g,t}^N\right|}{\left|P_{g,t}^P + \mathrm{j}Q_{g,t}^P\right|} \approx \frac{0.9375\max\left(\left|P_{g,t}^N\right|, \left|Q_{g,t}^N\right|\right) + 0.4688\min\left(\left|P_{g,t}^N\right|, \left|Q_{g,t}^N\right|\right)}{0.9375\max\left(\left|P_{g,t}^P\right|, \left|Q_{g,t}^P\right|\right) + 0.4688\min\left(\left|P_{g,t}^P\right|, \left|Q_{g,t}^P\right|\right)}, \quad (25a)$$

where:

$$P_{g,t}^N = P_{g,t}^a + \frac{\sqrt{3}}{2} Q_{g,t}^b - 0.5P_{g,t}^b - \frac{\sqrt{3}}{2} Q_{g,t}^c - 0.5P_{g,t}^c, \quad (25b)$$

$$Q_{g,t}^N = Q_{g,t}^a + \frac{\sqrt{3}}{2} P_{g,t}^c - 0.5Q_{g,t}^b - \frac{\sqrt{3}}{2} P_{g,t}^b - 0.5Q_{g,t}^c, \quad (25c)$$

$$P_{g,t}^P = P_{g,t}^a + P_{g,t}^b + P_{g,t}^c, \quad (25d)$$

$$Q_{g,t}^P = Q_{g,t}^a + Q_{g,t}^b + Q_{g,t}^c, \quad (25e)$$

$$P_{g,t}^a, P_{g,t}^b, P_{g,t}^c \in \mathbb{R}_{\ge 0}, Q_{g,t}^a, Q_{g,t}^b, Q_{g,t}^c \in \mathbb{R}. \quad (25f)$$

Equation (25a) can be linearized by introducing a series of binary variables and continuous variables, as shown in the APPENDIX. Then, the linear form of the DG current unbalance constraints can be described as:

$$0.9375y_{g,t}^{Nmax} + 0.4688y_{g,t}^{Nmin} \le CUF_g\big(0.9375y_{g,t}^{Pmax} + 0.4688y_{g,t}^{Pmin}\big), g \in \mathcal{G}^S \cap \mathcal{G}^{3\phi}, t \in \mathcal{T}, \quad (26)$$

where CUF_g is the maximum permissive CUF for DG g. $\mathcal{G}^{3\phi}$ is the set of three-phase DGs. Equation (26) guarantees each black-start DG operates securely under unbalanced operation conditions.

2) DG output constraints

$$x_{g,t}^G \cdot P_g^{min} \le \sum_{\phi\in\{a,b,c\}} P_{g,t}^{\phi} \le x_{g,t}^G \cdot P_g^{max},\ g \in \mathcal{G}, t \in \mathcal{T}, t > 1, \quad (27a)$$

$$x_{g,t}^G \cdot Q_g^{min} \le \sum_{\phi\in\{a,b,c\}} Q_{g,t}^{\phi} \le x_{g,t}^G \cdot Q_g^{max}, g \in \mathcal{G}, t \in \mathcal{T}, t > 1, \quad (27b)$$

$$0 \le \sum_{\phi\in\{a,b,c\}} P_{g,t}^{\phi} \le x_{g,t}^G \cdot P_g^{max}, g \in \mathcal{G}^S, t \in \mathcal{T},\ t = 1, \quad (27c)$$

$$0 \le \sum_{\phi\in\{a,b,c\}} P_{g,t}^{\phi} \le x_{g,t}^G \cdot P_g^{max}, g \in \mathcal{G}^S, t \in \mathcal{T},\ t = 1, \quad (27d)$$

$$P_{g,t}^a = P_{g,t}^b = P_{g,t}^c, Q_{g,t}^a = Q_{g,t}^b = Q_{g,t}^c, g \in \mathcal{G}\backslash\mathcal{G}^S, t \in \mathcal{T}, \quad (27e)$$

where P_g^{min}, P_g^{max}, Q_g^{min}, and Q_g^{max} are minimum and maximum values for active and reactive output of DG g. Equations (27c) – (27d) allow black start DGs to be started from a zero-loading condition. Equation (27e) requires that for non-black start DGs, the power generated by each phase should be the same.

3) DG ramp rate constraints

$$-x_{g,t}^G \cdot P_g^{RAMP} \cdot \Delta t \le \sum_{\phi\in\{a,b,c\}} P_{g,t}^{\phi} - \sum_{\phi\in\{a,b,c\}} P_{g,t-1}^{\phi} \le x_{g,t}^G \cdot P_g^{RAMP} \cdot \Delta t,\ g \in \mathcal{G}, t \in \mathcal{T}, t > 1, \quad (28)$$

where P_g^{RAMP} is the maximum ramp rate for DG g.

F. Connectivity Constraints

Connectivity constraints describe the physical connections among components including DGs, lines, loads, and buses.

1) DGs

$$x_{g,t}^G \le s_{g,t}^N,\quad g \in \mathcal{G}\backslash(\mathcal{G}^S \cup \mathcal{G}^F), t \in \mathcal{T}, \quad (29a)$$

$$x_{g,t}^G - x_{g,t-1}^G \ge 0,\ g \in \mathcal{G}, t \in \mathcal{T}, t > 1. \quad (29b)$$

Equation (29a) ensures that a dispatchable DG without black start capability should be started only when it connects to an energized node. Equation (29b) guarantees that once a DG is started, it cannot be tripped in the following steps. Equation (29b) is an optional constraint, which can be removed for DGs (e.g., renewables) that can be tripped after being started.

2) Lines

$$x_{ij,t}^{BR} \le s_{i,t}^N, x_{ij,t}^{BR} \le s_{j,t}^N, (i,j) \in \mathcal{B}^S\backslash\mathcal{B}^F, t \in \mathcal{T}, \quad (30a)$$

$$x_{ij,t}^{BR} = s_{i,t}^N, x_{ij,t}^{BR} = s_{j,t}^N, (i,j) \in \mathcal{B}\backslash(\mathcal{B}^S \cup \mathcal{B}^F), t \in \mathcal{T}, \quad (30b)$$

$$x_{ij,t}^{BR} - x_{ij,t-1}^{BR} \ge 0,\ (i,j) \in \mathcal{B}^S\backslash\mathcal{B}^F, t \in \mathcal{T}, t > 1. \quad (30c)$$

Equation (30a) require that if a switchable line is energized, both end nodes must be energized. Equations (30b) guarantee that a non-switchable line will be energized immediately when one of the end nodes is energized. Equation (30c) implies that a line cannot be tripped after being energized.

3) Loads

$$x_{l,t}^L \le s_{l,t}^N,\ l \in \mathcal{L}^S\backslash\mathcal{L}^F, t \in \mathcal{T}, \quad (31a)$$

$$x_{l,t}^L = s_{l,t}^N,\ l \in \mathcal{L}\backslash(\mathcal{L}^S \cup \mathcal{L}^F), t \in \mathcal{T}, \quad (31b)$$

$$x_{l,t}^L - x_{l,t-1}^L \ge 0,\ l \in \mathcal{L}^S, t \in \mathcal{T}, t > 1. \quad (31c)$$

Equation (31a) requires that a switchable load can only be energized when it connects to an energized node. Equation (31b) ensures a non-switchable load will be energized immediately when it connects to an energized node. Equation (31c) requires that if a load is restored, it cannot be tripped again.

G. Topological and Sequencing Constraints

Topological and sequencing constraints are defined to ensure that (1): each microgrid is isolated from other microgrids and operated in tree topology, and (2): all the lines are energized sequentially.

1) Concept of Bus Block

In a distribution system, some buses may be directly interconnected by non-switchable lines, thus forming a "bus block". Fig. 3 shows that by grouping buses into multiple bus blocks, the reduced network will only contain switchable lines. Each bus block contains at least one bus. Note that all the buses and lines within the same bus block will be energized at one time, which is guaranteed by (30b). For a reduced network, we denote $\mathcal{K} \coloneqq \{1,2,\dots,N_k\},\ N_k \le N_n$ as the set of bus blocks, and denote $\mathcal{C} \coloneqq \{(i,j): i \in \mathcal{K}, j \in \mathcal{K}, i \ne j\}$ as the switchable lines between bus blocks. $s_{k,t}^{BL}$ is defined as the energization status of bus block $k \in \mathcal{K}$ at step t. The energization status of a line $(i,j) \in \mathcal{C}$ can be represented by $x_{ij,t}^{BR}$.

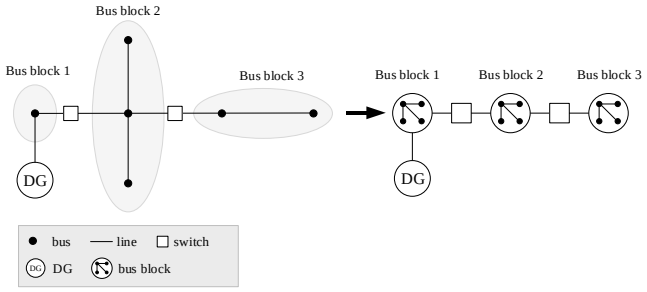

Fig. 3. The concept of "bus block," which can be formed by a single bus or multiple buses interconnected by non-switchable lines. The reduced network contains the switchable lines only.

2) Topology Constraints

Topology constraints ensure that each microgrid is isolated from other microgrids and operated in tree topology. For each bus i inside bus block k, we have:

$$s_{k,t}^{BL} = s_{i,t}^N, k \in \mathcal{K}, t \in \mathcal{T} \quad (32a)$$

Equation (32a) ensures that the energization status of each bus inside ~~a same~~ bus block k is represented by $s_{k,t}^{BL}$.

$$\big(s_{i,t}^{BL} - s_{i,t-1}^{BL}\big) + \big(s_{j,t}^{BL} - s_{j,t-1}^{BL}\big) \ge x_{(i,j),t}^{BR} - x_{(i,j),t-1}^{BR},\ (i,j) \in \mathcal{C}, t \in \mathcal{T}, t > 1, \quad (32b)$$

$$\sum_{i:\,(i,j)\in\mathcal{C}}\big(x_{ij,t}^{BR} - x_{ij,t-1}^{BR}\big) + \sum_{i:\,(k,i)\in\mathcal{C}}\big(x_{ki,t}^{BR} - x_{ki,t-1}^{BR}\big) \le 1 + M s_{i,t-1}^{BL}, i \in \mathcal{K}, t \in \mathcal{T}, t > 1. \quad (32c)$$

Equation (32b) requires that if both end bus blocks of a switchable line are already energized at step $t-1$, this line cannot be closed to avoid forming a loop. Equation (32c) ensures that if a bus block is de-energized at step $t-1$, then it can only be energized at step t by at most one switchable line.

3) Sequencing Constraints

Sequencing constraints guarantee that a feasible switching sequence can be generated and can be described by the following constraints:

$$s_{g,t}^N = x_{g,t}^G,\quad g \in \mathcal{G}^S\backslash\mathcal{G}^F, t \in \mathcal{T}, \quad (33a)$$

$$s_{i,t}^{BL} \le \sum_{i:\,(i,j)\in\mathcal{C}} x_{ij,t}^{BR} + \sum_{i:\,(k,i)\in\mathcal{C}} x_{ki,t}^{BR}, i \in \mathcal{K}, t \in \mathcal{T}, \quad (33b)$$

$$x_{(i,j),t}^{BR} \le s_{i,t-1}^{BL} + s_{j,t-1}^{BL},\quad (i,j) \in \mathcal{C}, t \in \mathcal{T}, t > 1. \quad (33c)$$

Equation (33a) ensures that a bus can be directly energized by a black start DG or a substation node. Then all the other buses inside the same bus block will be energized, according to (32a).

Equation (33b) ensures that a bus block can only be energized by an energized switchable line. Equation (33c) requires that each switchable line can only be energized when at least one of its end bus blocks is energized at the previous interval.

Furthermore, an optional constraint can be used to ensure that a set of loads (e.g., critical loads) can be restored prior to another set of loads:

$$x^{L}_{nl,t} \le x^{L}_{cl,t}, \quad cl, nl \in \mathcal{L}\backslash\mathcal{L}^{F}, t \in \mathcal{T}, \tag{33d}$$

where the subscript cl represents a particular critical load, and nl represents a particular non-critical load. Equation (33d) can be used for two or more loads that must be restored at a given sequence. Indeed, we can use (33d) to require that all the non-critical loads must be restored after all the critical loads are restored. Using (33d) may generate low-quality solutions. For example, if restoring a critical load cannot be restored due to limited operation margins, it will further prevent all the non-critical loads from being restored.

IV. Numerical Results

In this section, the proposed SSR algorithm is validated via the IEEE 123 node test feeder. The MILP problem is solved by CPLEX 12.6 on an Intel Core i7-4600U with a 2.1-GHz CPU, 12 GB of RAM, and 64-bit operating system PC.

A. IEEE 123 Node Test Feeder

The single-line diagram of the IEEE 123 node test feeder is shown in Fig. 4. Buses are represented by dots, and the substation bus (i.e., bus 150) is represented by a bar. Three-phase, two-phase, and single-phase lines are represented by black, yellow, and green wires, respectively. There are a total of 46 switchable lines and 4 voltage regulators in the system. Each voltage regulator is equipped with switches on both sides. Note that determining the optimal allocation for tie lines is beyond the scope of this paper. The detailed system parameters can be found in [41].

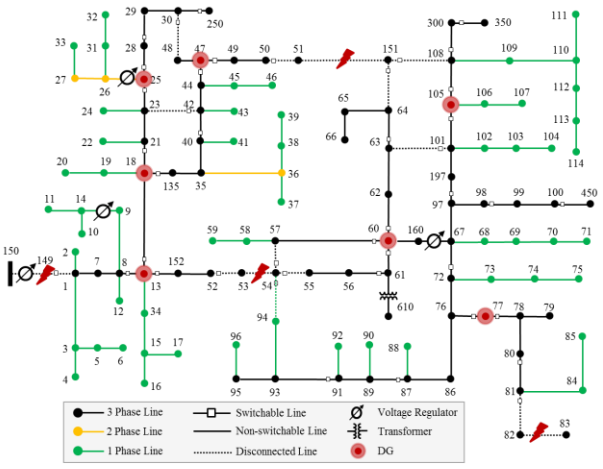

Fig. 4. IEEE 123 node test feeder with multiple DGs and tie switches.

Seven DGs are added to the system, and their parameters are summarized in TABLE I. "Status" indicates the type of DGs, where "1" indicates that the DG is a black start DG; "1/0" indicates that the DG is a non-black start DG but can be started by external sources; and "0" represents that the DG is not available for participating in the service restoration.

TABLE I
Parameters of DGs Added to IEEE 123 Node Test Feeder

Parameters	DG1	DG2	DG3	DG4	DG5	DG6	DG7
Node position	13	18	25	47	60	77	105
P_g^{max} (MW)	0.9	1.05	1.2	1.5	1.2	1.2	1.5
P_g^{min} (MW)	0.09	0.1	0.12	0.15	0.12	0.12	0.15
Q_g^{max} (MVar)	0.7	0.8	0.9	1.2	0.9	0.9	1.2
Q_g^{min} (MVar)	-0.5	-0.5	-0.6	-0.9	-0.6	-0.6	-0.9
P_g^{R}(MW/min)	0.5	0.4	0.3	0.2	0.3	0.5	0.6
CUF (%)	100%	20%	10%	10%	20%	10%	100%
MLS (%)	80%	70%	80%	60%	50%	60%	80%
Status	1	1	0	1/0	1	1/0	1

There are a total of 85 loads and 4 capacitors in the test system. The controllability is indicated in TABLE III, where a load is named by the letter "L" followed by a subscript and a bus number, and a capacitor is named by the letter "C" followed by a subscript and the bus number. For the sake of simplicity, the weight factor is assumed to be 1.0 for each load. If there are critical loads in the system, larger weight factors must be assigned to these critical loads, in order to restore them prior to other loads. The subscript "1" indicates that the load is directly connected to the bus, "1/0" indicates that the load can be remotely switched on or off, and "0" indicates that the load cannot be restored for some reasons. Switchable lines are named by the letter "S" with the superscript and the subscript as the "from bus" and "to bus", respectively.

Four permanent faults are applied to four locations, as shown in Fig. 4. Dashed lines indicate that these lines are opened in order to maintain the radial topology or isolate the faulty areas. For example, the fault occurring on line between Bus 53 and 54 (denoted as 53–54), which is in the middle of the feeder, should be isolated by opening the upstream switch (e.g., 52–53) and downstream switches (e.g., 54–57, 54–55, 54–94). A fault occurring on line 82–83, which is at the end of the feeder, should be isolated by opening the upstream switch (e.g., 81–82). Isolating the fault on line 150–1 will cause general blackout to the system. Tripped lines should keep being opened until the faulty areas are cleared. In this paper, the faults are assumed to be persisting during the restoration process.

For the sake of simplicity, the duration between two consecutive steps (i.e., Δt) is fixed to 1 minute. Properly setting up Δt is critical to accelerating the restoration process. Many factors should be considered, such as DG ramp rates, control delay, and transient responses. Determining Δt is out of the scope of this paper.

B. SSR Results

1) Impact of Horizon Lengths

Since the SSR method must define various variables and constraints for each step, it is important to decide a proper horizon length, or the total number of steps. In this paper, the horizon length used for presenting the case studies is set to 7. Note that the SSR method can only search for optimal solutions within a given horizon. Thus, different sequences may be generated when using different horizon lengths. On one hand, using large horizon lengths will require defining numerous variables and constraints; hence this requires extended computation time. On the other hand, using small horizon lengths may not guarantee the optimal solution for large-scale

systems. In this paper, different horizon lengths are tested. The total restored load at the end of the time horizon and computation time are summarized in TABLE II. TABLE II shows that only 1,704.8 kW of load are restored within three steps, and 3,143.5 kW of load are restored within five steps. When the horizon length is 7, 9, or 11, a total of 3,365.2 kW of load can be restored. This result indicates that choosing the horizon length to be 3 or 5 will generate only sub-optimal restoration solutions. However, the computation time increases exponentially as the horizon length is extended. Indeed, for large systems, solving the MILP model using large horizon lengths will become computationally intensive. Therefore, the horizon length should be determined carefully to balance the computation time and the quality of solutions. A proper horizon length can be determined offline, by solving various fault scenarios generated according to damage assessment reports. For online use, short horizon lengths can be selected to achieve satisfying results using the rolling-horizon method, which will be introduced later in this paper.

TABLE II
COMPUTATION TIME AND TOTAL RESTORED LOAD FOR DIFFERENT HORIZON LENGTHS

Horizon Length	Restored Load (kW)	Computation Time (s)
3	1704.8	2.59
5	3143.5	4.52
7	3365.2	9.88
9	3365.2	16.34
11	3365.2	30.82

2) Restoration Solution

The control sequence for switchable lines and loads is listed in TABLE III, given the horizon length is 7. Energized lines and voltage regulators are denoted by an upper-case letter "S" with a superscript representing one end bus, and a subscript representing the other end bus. At Step 1, 3 single-phase loads (i.e., $L_{1/0}16$, $L_{1/0}17$, and $L_{1/0}34$) are restored by DG1. This is because DG1 is inverter-based, hence it can operate at 100% CUF. At Step 7, a total of four loads cannot be restored because they are isolated due to the faults. Two voltage regulators on lines 150-149 and 160-67 are not energized.

As shown in Fig. 5, the system is partitioned into four isolated microgrids by energizing switchable lines sequentially, and the radial structure of each isolated microgrid is maintained at each step. Within each microgrid, all of the loads are balanced by the DGs within the same microgrid. It is worth noticing that two of the microgrids in Fig. 5 contains two DGs. For example, DG4 on Bus 47 is started at Step 4, according to TABLE III. Then, DG4 is coordinatively dispatched by the SSR method to generate designated amount of power during the following time steps.

Fig. 6 illustrates how one of the isolated microgrids in Fig. 5 is energized step-by-step by performing the restoration sequence. Note that only the first five steps are shown, since no more lines are energized after the fifth step. All of the energized lines are represented by solid black lines. At each step, all of the constraints including the radial topology and DG current unbalance constraints are satisfied.

TABLE III
SWITCHABLE LINES AND LOADS ENERGIZED AT EACH STEP

Step	Switched-on Lines	Restored Loads and DGs
1	None	{DG1, $L_{1/0}16$, $L_{1/0}17$, $L_{1/0}34$}[1], {DG2}[2], {DG5}[3], {DG7}[4]
2	$\{S_{13}^{8}, S_{152}^{13}\}^1$, $\{S_{21}^{18}, S_{135}^{18}\}^2$, $\{S_{60}^{57}, S_{61}^{60}, S_{62}^{60}\}^3$, $\{S_{105}^{101}, S_{108}^{105}\}^4$	{$L_1$1,$L_1$2,$L_1$4,$L_1$5,$L_1$6,$L_1$7,$L_1$9,$L_1$12,$L_1$52}[1],{$L_{1/0}$19,$L_{1/0}$20,$L_1$22,$L_1$24,$L_1$35,$L_1$37,$L_1$38, $L_1$39,$L_1$41}[2],{$L_1$58,$L_1$59,$L_{1/0}$60,$L_1$62, $L_1$63}[3], {$L_1$102,$L_1$103,$L_1$104, $L_{1/0}$106, $L_{1/0}$107,$L_1$109, $L_1$111, $L_1$112, $L_1$113, $L_1$114}[4]
3	$\{S_{14}^{9}\}^1$, $\{S_{25}^{23}, S_{42}^{40}\}^2$, $\{S_{64}^{63}, S_{61}^{56}\}^3$, $\{S_{197}^{97}\}^4$	{$L_1$10, $L_1$11}[1], {$L_1$43, $L_1$45}[2], {$L_1$64, $L_1$65, $L_1$66, $L_1$68, $L_1$69}[3], {$L_1$70, $L_1$71, $L_1$98}[4]
4	$\{S_{26}^{25}, S_{28}^{25}, S_{47}^{44}\}^2$, $\{S_{72}^{67}, S_{99}^{98}\}^4$	{DG4,$L_1$28,$L_1$31,$L_1$32,$L_1$33,$L_{1/0}$42,$L_{1/0}$46, $L_1$47,$L_1$48}[2], {$L_{1/0}$55, $L_{1/0}$56}[3], {$L_1$73,$L_1$74, $L_1$75,$L_1$76,$L_1$86, $L_1$87, $L_1$88, $L_1$99, $L_1$100}[4]
5	$\{S_{29}^{28}, S_{49}^{47}\}^2$, $\{S_{77}^{76}, S_{89}^{87}\}^4$	{$L_1$29, $L_1$30, $L_1$49, $L_1$50}[2], {DG6, $L_1$77, $L_1$90, $L_1$92}[4]
6	$\{S_{78}^{77}, S_{93}^{91}\}^4$	{$L_1$79,$L_1$80,$L_1$94,$L_1$95,$L_1$96,$C_{1/0}$89, $C_{1/0}$90}[4]
7	$\{S_{81}^{80}\}^4$	{$L_1$84, $L_1$85, $C_{1/0}$92}[4]
Loads Not Restored:		$L_0$51, $L_0$53, $L_0$82, $L_0$83

[a] Each isolated microgrid is denoted by {■}[No.]. 'No.' is the index of formed microgrids. The components energized by each microgrid are denoted in the bracket.

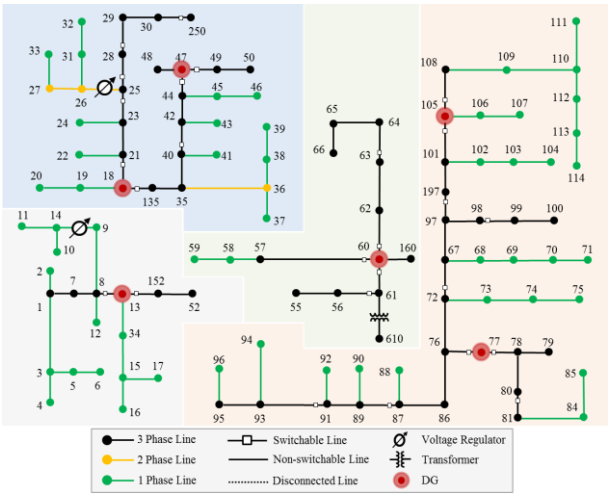

Fig. 5. Energized system at the last step. De-energized components are removed from the original diagram. Four isolated microgrids are formed.

The three-phase voltage for each bus at the last step (i.e., seventh step) is shown in Fig. 7. Each vertically aligned column of dots represents the phase voltages on one bus. Note that some nodal voltages are not shown because they are not energized. For single-phase or two-phase buses, one or two dots corresponding to the associated phases will be present in the vertically aligned columns. The phase voltages for all of the energized buses fall between 0.985 p.u. to 1.01 p.u. In addition, the phase voltage constraints are satisfied for each step but are not shown owing to space limitations.

Fig. shows the three-phase active power output for each DG at each step. Black start DGs (i.e., DG1, DG2, DG5, and DG7) are operated under unbalanced condition to balance the load demand on each phase, whereas non-black start DGs (i.e., DG4 and DG6) are dispatched to output same amount of power to each phase. DG3 is not started.

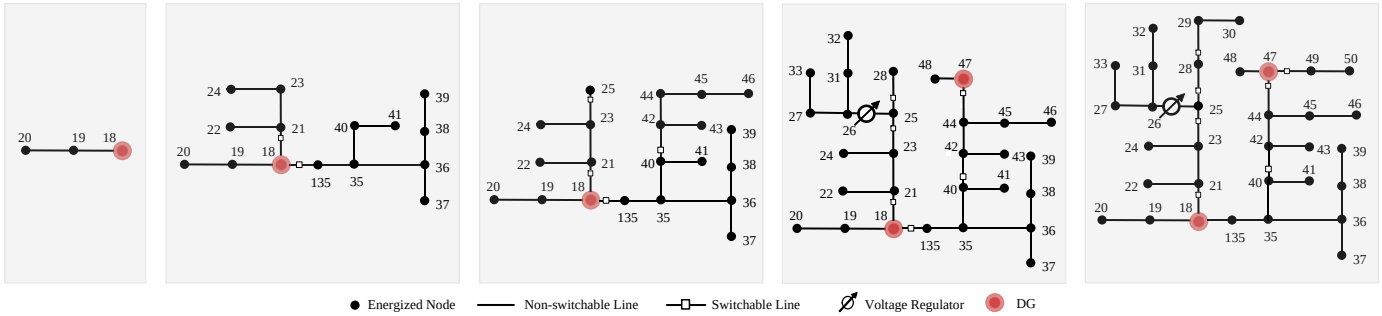

Fig. 6. Single-line diagram to demonstrate how one of the isolated microgrids is developed step-by-step. Only configurations for the first five steps are shown, since no more lines and loads are energized after the fifth step. Only energized lines are shown.

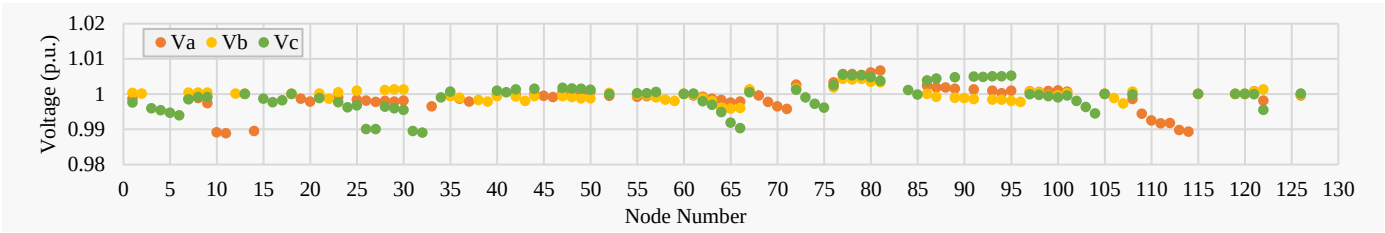

Fig. 7. Three-phase nodal voltage at the last step. System nodes are numbered in ascending order based on their original names. Vertically aligned dots represent associated phase voltages on the same bus. Only energized nodal voltages are shown.

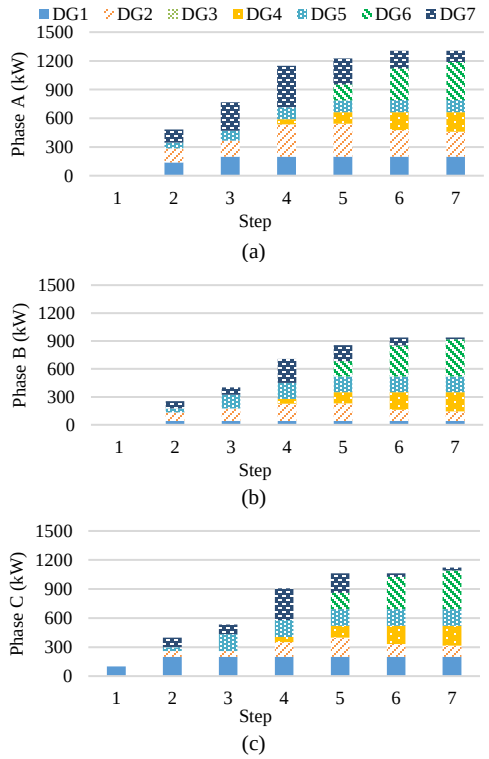

Fig. 8. Active power output of each DG at each step: (a) phase A active power output, (b) phase B active power output, (c) phase C active power output.

3) Rolling-horizon method

The proposed SSR method can be initiated from any operational conditions, so it can be easily configured to implement the rolling-horizon method. In the rolling-horizon method, we can repeatedly run the SSR algorithm by incorporating the system configuration from the previous iteration as the initial condition for the current iteration. For each iteration, the horizon length will be fixed. This process will continue until no more loads can be restored.

TABLE IV summarizes the computation time and total restored energy using different horizon lengths in the rolling-horizon method. For each selected horizon length, no more loads will be restored after the ninth step, which allows us to compare the total energy restored within the first nine steps and the restored load demand at Step 9. According to TABLE IV, all the selected horizon lengths can eventually restore 3,365.2 kW of load demand using the rolling-horizon method at Step 9. Using smaller horizon lengths (e.g., 3 and 5) requires less computation time and more iterations than using larger horizon lengths (e.g., 11). In terms of total restored energy, smaller horizon lengths may generate suboptimal solutions. For example, when the horizon length is set to 3, 368.37 kWh is restored within nine steps. However, the rest of the selected horizon lengths can lead to restoring 371.13 kWh within nine steps. This is because for each iteration, the SSR method will only search for the optimal solution within the given horizon length. Therefore, smaller horizon lengths can be easily trapped in local optimal solutions, due to lack of coordination across multiple steps. Fig. 9 shows the total restored load at each step for different horizon lengths. At Step 4, less load is restored when the horizon length is 3. This is because during the first iteration (i.e., Step 1 through Step 3), the SSR method generated a restoration sequence that prevents more loads from being restored during the second iteration (i.e., Step 3 to Step 5).

TABLE IV
COMPUTATION TIME AND TOTAL RESTORED ENERGY FOR DIFFERENT HORIZON LENGTHS USING ROLLING-HORIZON METHOD

Horizon Length	No. of Iteration	Total Energy Restored Within 9 Steps (kWh)	Restored Load at 9th Step (kW)	Computation Time (s)
3	5	368.37	3365.2	10.15
5	3	371.13	3365.2	11.31
7	2	371.13	3365.2	15.04
9	1	371.13	3365.2	16.34
11	1	371.13	3365.2	30.82

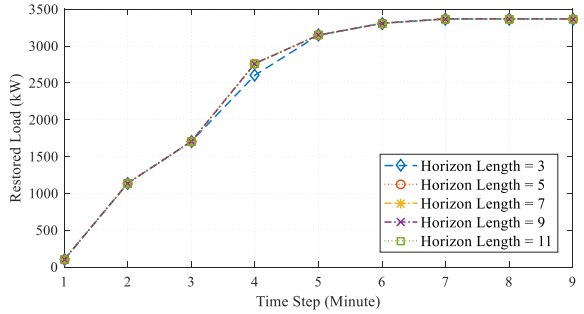

Fig. 9. Restored load demand at each step for different horizon lengths

C. Solution Validation

The linear three-phase power flow used in the MILP model can approximate the voltage and line power for three-phase unbalanced systems, but inevitably introduces approximation errors. In this paper, the restoration solution generated by the SSR method is validated by OpenDSS, which is an open-source software developed by the Electric Power Research Institute (EPRI). Multiple testing scenarios are generated based on the modified IEEE 123 node system for validation purposes. The load profile is enlarged by a scale factor between 1.0 and 1.5. For each scenario, a restoration sequence is generated using the SSR method. For each restoration sequence, at each step, the linear power flow results are compared with the OpenDSS results in the correlation plots, as shown in Fig. 10. In Fig. 10(a), voltage magnitudes derived from the MILP model are compared with OpenDSS results. It shows that the voltage magnitudes are always maintained between 0.98 p.u. and 1.02 p.u., and that they are closely correlated with the OpenDSS results. The maximum error is around 0.002 p.u. In Fig. 10(b), the line apparent powers approximated by the linear power flow are compared with the OpenDSS results. The maximum error is around 80 kVA. This is mainly due to the fact that the nonlinear terms, which represent the system losses and voltage drops, are neglected in the linear power flow model. Since the power outputs of non-black start DGs are the same for both linear and nonlinear models, black start DGs in the nonlinear power flow model will produce more power to account for the system losses. Therefore, some lines may be overloaded in OpenDSS if they are already fully loaded in the linear power flow model. Conservative limits can be used to avoid violating the line capacity constraints.

V. Conclusion

In this paper, a novel SSR methodology is proposed for restoring unbalanced distribution systems and microgrids. The SSR problem is formulated as a MILP model, which can efficiently generate the optimal restoration sequences to coordinate dispatchable DGs and switchgears to energize the system on a step-by-step basis. The SSR methodology can adapt to various operation conditions and form multiple isolated subsystems, while satisfying self-adequacy and operation constraints for each subsystem. The rolling-horizon method is further employed to reduce the extensive computation complexity for large-scale systems.

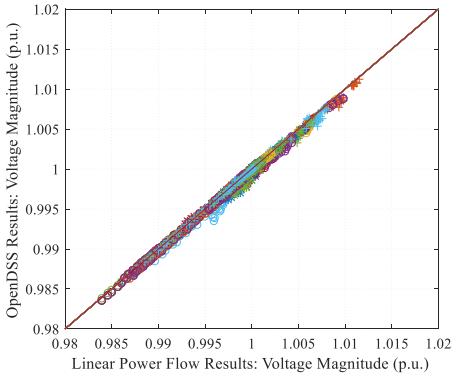

(a)

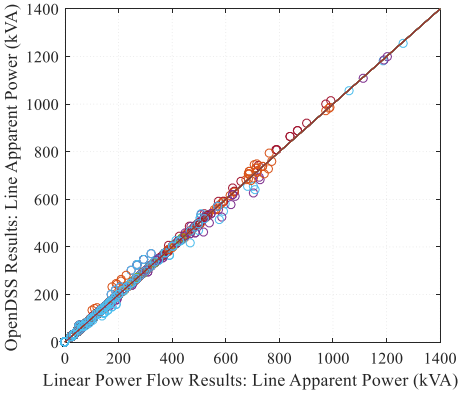

(b)

Fig. 10. Correlation between linear power flow results and OpenDSS results

Appendix

This appendix provides the derivation of the linear approximation of the nonlinear terms in equation (25a) in Section III.*D*. Define $y_{g,t}^{PN}, y_{g,t}^{QN}, y_{g,t}^{PP}, y_{g,t}^{QP} \in \mathbb{R}^{T\times n_g}$, and $d_{g,t}^{PN1}$, $d_{g,t}^{PN2}, d_{g,t}^{QN1}, d_{g,t}^{QN2}, d_{g,t}^{QP1}$, $d_{g,t}^{QP2} \in \{0,1\}^{T\times n_g}$, then $\left|P_{g,t}^{N}\right|$, $\left|Q_{g,t}^{N}\right|$, $\left|P_{g,t}^{P}\right|$ and $\left|Q_{g,t}^{P}\right|$ can be linearized by:

$$0 \le y_{g,t}^{PN} - P_{g,t}^{N} \le U_g^{max} d_{g,t}^{PN1}, \quad (34a)$$
$$0 \le y_{g,t}^{PN} + P_{g,t}^{N} \le U_g^{max} d_{g,t}^{PN2}, \quad (34b)$$
$$d_{g,t}^{PN1} + d_{g,t}^{PN2} = 1, \quad (34c)$$
$$0 \le y_{g,t}^{QN} - Q_{g,t}^{N} \le U_g^{max} d_{g,t}^{QN1}, \quad (34d)$$
$$0 \le y_{g,t}^{QN} + Q_{g,t}^{N} \le U_g^{max} d_{g,t}^{QN2}, \quad (34e)$$
$$d_{g,t}^{QN1} + d_{g,t}^{QN2} = 1, \quad (34f)$$
$$y_{g,t}^{PP} = P_{g,t}^{P}, \quad (34g)$$
$$0 \le y_{g,t}^{QP} - Q_{g,t}^{P} \le 2U_g^{max} d_{g,t}^{QP1}, \quad (34h)$$
$$0 \le y_{g,t}^{QP} + Q_{g,t}^{P} \le 2U_g^{max} d_{g,t}^{QP2}, \quad (34i)$$
$$d_{g,t}^{QP1} + d_{g,t}^{QP2} = 1, \quad (34j)$$
$$g \in \mathcal{G}, t \in \mathcal{T}, \quad (34k)$$

where $U_g^{max} = P_g^{max} + Q_g^{max}$.

Define $y_{g,t}^{Nmax}, y_{g,t}^{Nmin} \in \mathbb{R}^{T\times n_g}$, $d_{g,t}^{Nmax1}$, $d_{g,t}^{Nmax2}$, $d_{g,t}^{Nmin1}$, $d_{g,t}^{Nmin2} \in \{0,1\}^{T\times n_g}$, then $\max\left(y_{g,t}^{PN}, y_{g,t}^{QN}\right)$ and $\min\left(y_{g,t}^{PN}, y_{g,t}^{QN}\right)$ can be linearized as:

$$y_{g,t}^{Nmax} \ge y_{g,t}^{PN}, y_{g,t}^{Nmax} \ge y_{g,t}^{QN}, \quad (35a)$$
$$y_{g,t}^{Nmax} \le y_{g,t}^{PN} + U_g^{max}\left(1 - d_{g,t}^{Nmax1}\right), \quad (35b)$$
$$y_{g,t}^{Nmax} \le y_{g,t}^{QN} + U_g^{max}\left(1 - d_{g,t}^{Nmax2}\right), \quad (35c)$$
$$d_{g,t}^{Nmax1} + d_{g,t}^{Nmax2} = 1, g \in \mathcal{G}, t \in \mathcal{T}. \quad (35d)$$

$$y_{g,t}^{Nmin} \le y_{g,t}^{PN}, y_{g,t}^{Nmin} \le y_{g,t}^{QN}, \quad (35e)$$

$$y_{g,t}^{Nmin} \ge y_{g,t}^{PN} - P_g^{max}\left(1 - d_{g,t}^{Nmin1}\right), \quad (35f)$$

$$y_{g,t}^{Nmin} \ge y_{g,t}^{QN} - Q_g^{max}\left(1 - d_{g,t}^{Nmin2}\right), \quad (35g)$$

$$d_{g,t}^{Nmin1} + d_{g,t}^{Nmin2} = 1, g \in \mathcal{G}, t \in \mathcal{T}. \quad (35h)$$

Similarly, $\max\left(y_{g,t}^{PP}, y_{g,t}^{QP}\right)$ and $\min\left(y_{g,t}^{PP}, y_{g,t}^{QP}\right)$ can be linearized by introducing $y_{g,t}^{Pmax}$, $y_{g,t}^{Pmin} \in \mathbb{R}^{T \times n_g}$, $d_{g,t}^{Pmax1}$, $d_{g,t}^{Pmax2}$, $d_{g,t}^{Pmin1}$, $d_{g,t}^{Pmin2} \in \{0,1\}^{T \times n_g}$:

$$y_{g,t}^{Pmax} \ge y_{g,t}^{PP}, y_{g,t}^{Pmax} \ge y_{g,t}^{QP}, \quad (36a)$$

$$y_{g,t}^{Pmax} \le y_{g,t}^{PP} + U_g^{max}\left(1 - d_{g,t}^{Pmax1}\right), \quad (36b)$$

$$y_{g,t}^{Pmax} \le y_{g,t}^{QP} + U_g^{max}\left(1 - d_{g,t}^{Pmax2}\right), \quad (36c)$$

$$d_{g,t}^{Pmax1} + d_{g,t}^{Pmax2} = 1, g \in \mathcal{G}, t \in \mathcal{T}. \quad (36d)$$

$$y_{g,t}^{Pmin} \le y_{g,t}^{PP}, y_{g,t}^{Pmin} \le y_{g,t}^{QP}, \quad (36e)$$

$$y_{g,t}^{Pmin} \ge y_{g,t}^{PP} - P_g^{max}\left(1 - d_{g,t}^{Pmin1}\right), \quad (36f)$$

$$y_{g,t}^{Pmin} \ge y_{g,t}^{QP} - Q_g^{max}\left(1 - d_{g,t}^{Pmin2}\right), \quad (36g)$$

$$d_{g,t}^{Pmin1} + d_{g,t}^{Pmin2} = 1, g \in \mathcal{G}, t \in \mathcal{T}. \quad (36h)$$

ACKNOWLEDGEMENT

J. Wang's work is supported by the U.S. Department of Energy (DOE)'s Office of Electricity Delivery and Energy Reliability.

REFERENCES

[1] R. J. Campbell, Weather-related power outages and electric system resiliency: Congressional Research Service, Library of Congress, 2012.

[2] Y. Wang, C. Chen, J. Wang and R. Baldick, "Research on resilience of power systems under natural disasters—a review," in *IEEE Transactions on Power Systems*, vol. 31, no. 2, pp. 1604-1613, March 2016.

[3] B. Chen, S. Mashayekh, K. L. Butler-Purry and D. Kundur, "Impact of cyber attacks on transient stability of smart grids with voltage support devices," *2013 IEEE Power & Energy Society General Meeting*, Vancouver, BC, 2013, pp. 1-5.

[4] S. Liu, B. Chen, T. Zourntos, D. Kundur and K. Butler-Purry, "A coordinated multi-switch attack for cascading failures in smart grid," in *IEEE Transactions on Smart Grid*, vol. 5, no. 3, pp. 1183-1195, May 2014.

[5] B. Renz, J. Miller, and J. Harmon, "Anticipates and responds to system disturbances (self-heals)," National Energy Technology Laboratory, U.S. Department of Energy DOE/NETL-2010/1421, August 2010.

[6] —, "A systems view of the Modern Grid: Appendix A1 Self-Heals," the National Energy Technology Laboratory, U.S. Department of Energy, 2007.

[7] C. Abbey, D. Cornforth, N. Hatziargyriou, K. Hirose, A. Kwasinski, E. Kyriakides, et al., "Powering Through the Storm: Microgrids Operation for More Efficient Disaster Recovery," in *IEEE Power and Energy Magazine*, vol. 12, no. 3, pp. 67-76, May-June 2014.

[8] H. Ahmadi, A. Alsubaie and J. R. Martí, "Distribution system restoration considering critical infrastructures interdependencies," *2014 IEEE PES General Meeting | Conference & Exposition*, National Harbor, MD, 2014, pp. 1-5.

[9] Qin Zhou, D. Shirmohammadi and W. H. E. Liu, "Distribution feeder reconfiguration for service restoration and load balancing," in *IEEE Transactions on Power Systems*, vol. 12, no. 2, pp. 724-729, May 1997.

[10] S. Khushalani, J. M. Solanki and N. N. Schulz, "Optimized restoration of unbalanced distribution systems," in *IEEE Transactions on Power Systems*, vol. 22, no. 2, pp. 624-630, May 2007.

[11] K. L. Butler-Purry and N. D. R. Sarma, "Self-healing reconfiguration for restoration of naval shipboard power systems," in *IEEE Transactions on Power Systems*, vol. 19, no. 2, pp. 754-762, May 2004.

[12] J. Li, X. Y. Ma, C. C. Liu and K. P. Schneider, "Distribution system restoration with microgrids using spanning tree search," in *IEEE Transactions on Power Systems*, vol. 29, no. 6, pp. 3021-3029, Nov. 2014.

[13] S. Mohagheghi and F. Yang, "Applications of microgrids in distribution system service restoration," 2011 *Innovative Smart Grid Technologies (ISGT)*, Hilton Anaheim, CA, 2011, pp. 1-7.

[14] B. Ansari and S. Mohagheghi, "Electric service restoration using microgrids," *2014 IEEE PES General Meeting | Conference & Exposition*, National Harbor, MD, 2014, pp. 1-5.

[15] T. T. H. Pham, Y. Besanger and N. Hadjsaid, "New challenges in power system restoration with large scale of dispersed generation insertion," in *IEEE Transactions on Power Systems*, vol. 24, no. 1, pp. 398-406, Feb. 2009.

[16] C. Chen, J. Wang, F. Qiu and D. Zhao, "Resilient distribution system by microgrids formation after natural disasters," in *IEEE Transactions on Smart Grid*, vol. 7, no. 2, pp. 958-966, March 2016.

[17] Z. Wang and J. Wang, "Self-healing resilient distribution systems based on sectionalization into microgrids," in *IEEE Transactions on Power Systems*, vol. 30, no. 6, pp. 3139-3149, Nov. 2015.

[18] A. Sharma, D. Srinivasan and A. Trivedi, "A decentralized multiagent system approach for service restoration using DG islanding," in *IEEE Transactions on Smart Grid*, vol. 6, no. 6, pp. 2784-2793, Nov. 2015.

[19] H. Li, A. T. Eseye, J. Zhang, and D. Zheng, "Optimal energy management for industrial microgrids with high-penetration renewables," *Protection and Control of Modern Power Systems*, vol. 2, pp. 12-28, 2017.

[20] I. Watanabe and M. Nodu, "A genetic algorithm for optimizing switching sequence of service restoration in distribution systems," *Proceedings of the 2004 Congress on Evolutionary Computation* (IEEE Cat. No.04TH8753), 2004, pp. 1683-1690.

[21] R. Perez-Guerrero, G. T. Heydt, N. J. Jack, B. K. Keel and A. R. Castelhano, "Optimal restoration of distribution systems using dynamic programming," in *IEEE Transactions on Power Delivery*, vol. 23, no. 3, pp. 1589-1596, July 2008.

[22] S. Thiébaux, C. Coffrin, H. Hijazi, and J. Slaney, "Planning with MIP for supply restoration in power distribution systems," presented at *the Proceedings of the Twenty-Third international joint conference on Artificial Intelligence*, Beijing, China, 2013.

[23] C. Coffrin and P. Van Hentenryck, "Transmission system restoration with co-optimization of repairs, load pickups, and generation dispatch," *International Journal of Electrical Power & Energy Systems*, vol. 72, pp. 144-154, Nov. 2015.

[24] S. Borlase, *Smart Grids: Infrastructure, Technology, and Solutions*: Taylor & Francis, 2012.

[25] W. H. Kersting, *Distribution System Modeling and Analysis*: CRC Press, 2001.

[26] S. Srivastava and K. L. Butler-Burry, "Expert-system method for automatic reconfiguration for restoration of shipboard power systems," in *IEE Proceedings - Generation, Transmission and Distribution*, vol. 153, no. 3, pp. 253-260, 11 May 2006.

[27] D. Kleppinger, R. Broadwater, and C. Scirbona, "Generic reconfiguration for restoration," *Electric Power Systems Research*, vol. 80, no. 3, pp. 287-295, March 2010.

[28] H. Ahmadi, J. R. Martı´ and A. von Meier, "A linear power flow formulation for three-phase distribution systems," in *IEEE Transactions on Power Systems*, vol. 31, no. 6, pp. 5012-5021, Nov. 2016.

[29] L. Gan and S. H. Low, "Convex relaxations and linear approximation for optimal power flow in multiphase radial networks," *2014 Power Systems Computation Conference*, Wroclaw, 2014, pp. 1-9.

[30] B. A. Robbins and A. D. Domínguez-García, "Optimal reactive power dispatch for voltage regulation in unbalanced distribution systems," in *IEEE Transactions on Power Systems*, vol. 31, no. 4, pp. 2903-2913, July 2016.

[31] A. Borghetti, F. Napolitano, and C. A. Nucci, "Volt/var optimization of unbalanced distribution feeders via mixed integer linear programming," *International Journal of Electrical Power & Energy Systems*, vol. 72, pp. 40-47, Nov. 2015.

[32] Z. Wang; J. Wang; C. Chen, "A three-phase microgrid restoration model considering unbalanced operation of distributed generation," in *IEEE Transactions on Smart Grid* , vol.PP, no.99, pp.1-1.

[33] P. P. Barker and R. W. De Mello, "Determining the impact of distributed generation on power systems. Part I - Radial distribution systems," *2000 Power Engineering Society Summer Meeting* (Cat. No.00CH37134), Seattle, WA, 2000, pp. 1645-1656 vol. 3.

[34] R. E. Brown, *Electric power distribution reliability*: CRC press, 2008.

[35] J. A. Taylor and F. S. Hover, "Convex models of distribution system reconfiguration," in *IEEE Transactions on Power Systems*, vol. 27, no. 3, pp. 1407-1413, Aug. 2012.

[36] B. A. Robbins, H. Zhu and A. D. Domínguez-García, "*Optimal tap setting of voltage regulation transformers in unbalanced distribution systems*," in IEEE Transactions on Power Systems, vol. 31, no. 1, pp. 256-267, Jan. 2016.

[37] J. F. Franco, M. J. Rider, M. Lavorato, and R. Romero, "A mixed-integer LP model for the optimal allocation of voltage regulators and capacitors in radial distribution systems," *International Journal of Electrical Power & Energy Systems*, vol. 48, pp. 123-130, June 2013.
[38] M. Adibi et al., "Power system restoration - A task force report," in *IEEE Transactions on Power Systems*, vol. 2, no. 2, pp. 271-277, May 1987.
[39] M. W. Davis, R. Broadwater, and J. Hambrick, "Modeling and testing of unbalanced loading and voltage regulation: Final report," National Renewable Energy Laboratory, Golden, CO, USA, Subcontract Rep. NREL/SR-581-41805, July 2007.
[40] M. Allie and R. Lyons, "A root of less evil [digital signal processing]," in *IEEE Signal Processing Magazine*, vol. 22, no. 2, pp. 93-96, March 2005.
[41] IEEE PES Distribution Test Feeders [Online]. Available: http://www.ewh.ieee.org/soc/pes/dsacom/testfeeders/index.html

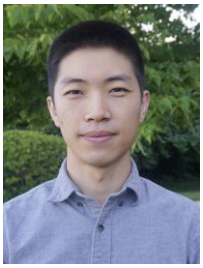

Bo Chen (M'17) received the Ph.D. degree in electrical engineering from Texas A&M University, College Station, USA, in 2017. He recived the B.S. and M.S. degrees from North China Electric Power University, Baoding, China. In 2016, he worked as a research aide at the Argonne National Laboratory, IL, USA. Currently, he is a postdoctoral researcher at the Energy Systems Division, Argonne National Laboratory, IL, USA. His research interests include modeling, control, and optimization of power systems, and co-simulation of cyber-physical smart grids.

Chen Chen (M'13) received the B.S. and M.S. degrees from Xi'an Jiaotong University, Xi'an, China, in 2006 and 2009, respectively, and the Ph.D. degree in electrical engineering from Lehigh University, Bethlehem, PA, USA, in 2013. During 2013-2015, he worked as a postdoctoral researcher at the Energy Systems Division, Argonne National Laboratory, Argonne, IL, USA. Dr. Chen is currently a Computational Engineer with the Energy Systems Division at Argonne National Laboratory. His primary research is in optimization, communications and signal processing for smart electric power systems, cyber-physical system modeling for smart grids, and power system resilience.

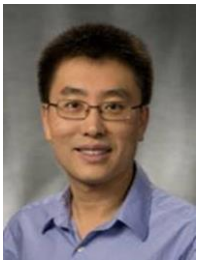

Jianhui Wang (M'07-SM'12) received the Ph.D. degree in electrical engineering from Illinois Institute of Technology, Chicago, Illinois, USA, in 2007.
Presently, he is an Associate Professor with the Department of Electrical Engineering at Southern Methodist University, Dallas, Texas, USA. He also holds a joint appointment as Section Lead for Advanced Power Grid Modeling at the Energy Systems Division at Argonne National Laboratory, Argonne, Illinois, USA.
Dr. Wang is the secretary of the IEEE Power & Energy Society (PES) Power System Operations, Planning & Economics Committee. He is an associate editor of Journal of Energy Engineering and an editorial board member of Applied Energy. He has held visiting positions in Europe, Australia and Hong Kong including a VELUX Visiting Professorship at the Technical University of Denmark (DTU). Dr. Wang is the Editor-in-Chief of the IEEE Transactions on Smart Grid and an IEEE PES Distinguished Lecturer. He is also the recipient of the IEEE PES Power System Operation Committee Prize Paper Award in 2015.

Karen L. Butler-Purry received the B.S. degree (summa cum laude) in Electrical Engineering from Southern University, USA, the M.S. degree from the University of Texas at Austin, USA, and the Ph.D. degree in Electrical Engineering from Howard University, USA. She joined Texas A&M University, USA, in 1994, where she currently serves as Interim Vice President for Research and Professor in the Department of Electrical and Computer Engineering. Her research interests are in the areas of protection and control of distribution systems and isolated power systems such as all electric power systems for ships, mobile grids, and microgrids, cybersecurity protection, intelligent systems for equipment deterioration and fault diagnosis, and engineering education.